Eur. J. Mineral.
2006, **18**, 187–195

Transformation of natural As-associated ferrihydrite downstream of a remediated mining site

JÉRÔME GAUTIER*, CÉCILE GROSBOIS, ALEXANDRA COURTIN-NOMADE, JEAN PIERRE FLOC'H and FRANÇOIS MARTIN

Laboratoire HydrASA, équipe ETM, UMR 6532 CNRS, Université de Limoges, Faculté des Sciences,
123 Avenue Albert Thomas, 87060 Limoges cedex, France
*Corresponding author, e-mail: jerome.gautier@unilim.fr

Abstract: Natural ferrihydrite (Fh), a poorly crystalline iron oxy-hydroxide with high concentrations of As, was investigated with respect to its crystallinity in a remediated mining environment. The Fh crystallinity increases from proto-Fh to a better crystallized 2-line Fh (called better 2-line Fh), while the associated As contents decrease from 7.8 to 1.9 wt %, respectively. This evolution of crystallinity correlated with decreasing As suggests that As is more likely coprecipitated in the Fh structure than adsorbed onto the surface.

The evolution of Fh crystallinity is related to (i) aqueous transformations for samples continuously submerged and controlled by water composition (pH, ionic strength and redox potential) and (ii) dry thermal transformations for samples in a seasonally humid area with variations of temperature, humidity, agglomeration and compaction. The evolution of Fh crystallinity is more pronounced during dry thermal transformation than during aqueous transformations. Although Fh evolution is observed on the field, no stable form (goethite, hematite) is detected as usually noted during dry thermal transformation. This may be explained by incorporated cations such as Si and Al that can inhibit the transformation of Fh to a more stable form. To understand this transformation in a natural environment, the discussion in this study focuses on two main points: (i) the relationship between spatial mineralogical distribution and As content and (ii) the importance of Fh evolution as a function of transformation processes observed in the field.

Key-words: ferrihydrite, arsenic, crystallinity transformation.

Introduction

Ferrihydrite (Fh), an iron (III) oxide (formula $5Fe_2O_3 \cdot 9H_2O$; Eggleton & Fitzpatrick, 1988), is typically encountered in mine drainage environments with pH values exceeding 5 (Carlson *et al.*, 2002). Fh is one of the most common secondary iron phases, along with its transformation products, goethite and hematite, and it is generally classified according to the number of X-ray diffraction lines (Cornell & Schwertmann, 1996). Typically, the "2-line Fh" shows two broad peaks corresponding to a poorly crystalline material, while the "6-line Fh" shows 6 finer peaks corresponding to a more highly crystalline material (Cornell & Schwertmann, 1996; Jambor & Dutrizac, 1998). The least crystalline Fh, also called "poorly 2-line Fh" or proto-ferrihydrite (Chukhrov, 1973; Cornell & Schwertmann, 1996), generally precipitates first. The structural model of Fh still remains a matter of debate due to the poor crystallinity of Fh. It may correspond to either (i) iron (III) sheets that are only octahedrally coordinated (Manceau, 1995) or (ii) iron (III) sheets that are both octahedrally and tetrahedrally coordinated (Eggleton & Fitzpatrick, 1988; Drits *et al.*, 1993).

Aqueous parameters such as pH, ionic strength and redox potential can prevent the evolution from poorly to more highly crystalline Fh (Cornell & Schwertmann, 1979; Torrent & Guzman, 1982; Vempati & Loeppert, 1989; Martinez & McBride, 1999 and Jang *et al.*, 2003). These parameters can be responsible for the transformation of Fh to other crystalline iron oxides (goethite and hematite). Cations and organic anions present in the structure can also modify the Fh properties (Schwertmann, 1979; Karim, 1984; Waychunas *et al.*, 1993 and Manceau, 1995). As an example, Zhao *et al.* (1994) showed that the transformation of silica-bearing Fh into hematite required higher temperature than for non silica-bearing Fh. Thus, all of the cited parameters are responsible for the dry thermal or aqueous transformation of Fh into a more crystalline oxide, as discussed by Jambor & Dutrizac (1998). Indeed, pH and ionic strength are involved during the aqueous transformation of Fh, whereas dryness, agglomeration and compaction are responsible for its dry thermal transformation.

Fh particles have a large specific surface area (> 220 m^2/g) and are therefore good adsorbents in aquatic systems, playing a crucial role in the bioavailability and migration behaviour of trace elements (TE) (Appelo *et al.*, 2002; Fuller *et al.*, 1993; Waychunas *et al.*, 1993). Concern-

DOI: 10.1127/0935-1221/2006/0018-0187
0935-1221/06/0018-0187 $ 4.05

ing arsenic, Fh shows properties that reflect a high sorption affinity for both As (III) and As (V) (Appelo *et al.*, 2002; Bigham *et al.*, 1996; Dold, 2003; Rancourt *et al.*, 2001). Consequently, Fh crystallinity is able to control As cycling in natural environments. The relevance of this study consists in observing the evolution of natural Fh precipitates according to *in situ* conditions and the decrease in As content downstream of a remediated mining site. This study allows us to forecast the short- and long-term risks of potential As pollution.

Materials and methods

Study area

The Saint-Yrieix gold mining district, one of the most important in France during the last century, is located in the northwestern part of the French Massif Central, near Limoges (Fig. 1). The mining of gold started in ancient times with the Celts (500 BC), and continued intermittently up until 2001, producing an estimated total of 55 metric tonnes of gold (Nicaud, 2001). The mineralized veins crosscut ortho- and paragneisses, and consist of quartz hosting arsenopyrite, pyrite, galena and sulpho-salts (Bouchot *et al.*, 1989; Cathelineau *et al.*, 1989).

The study area is located in the flood plain of the Manaurie river in the Dordogne basin (Fig. 1). Mining activities favoured groundwater circulation, leaching pyrite and arsenopyrite deposits coming from the quartz vein. The sampling site corresponds to a recently precipitated ochreous deposit covering 500 m^2, which results from the resurgence of groundwaters. The seepages of resurgent groundwater yield

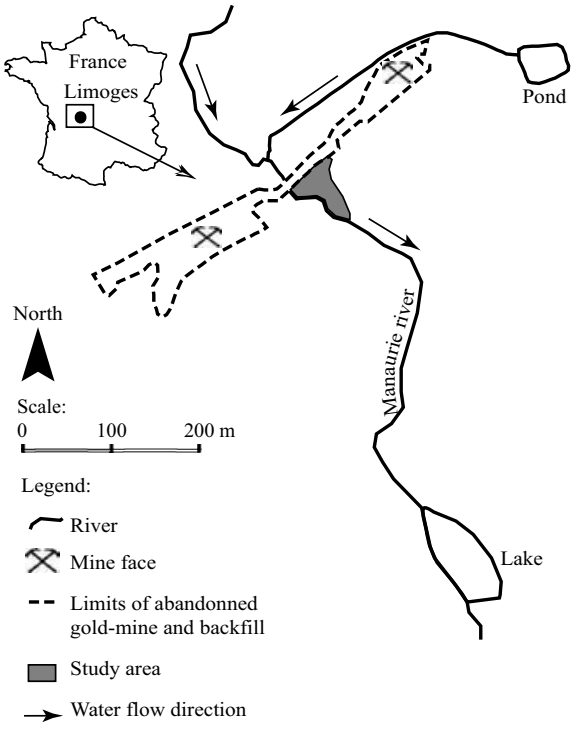

Fig. 1. Location of the studied area.

mean dissolved O_2 concentrations of 2.6 ± 2.4 mg/l and pH = 5.9 ± 0.3 (n = 37), with calcium sulphate and dissolved As concentrations ranging between 1.0 and 6.1 µM (this study). Ochreous deposits are located (i) in a drain built by miners to evacuate waters towards the local river and (ii) in 3–5-cm thick layers outside the drain (Fig. 2).

Sample collection and preparation

Ochreous deposits were collected along the main drain (samples a, b and c, Fig. 2), in a seasonal pool area (sample d, Fig. 2) and along the orthogonal drain (sample e, Fig. 2). Samples were collected using a manual vacuum-pump system, then acidified, placed in high-density polypropylene bottles and stored at 4°C. The Eh, pH, conductivity, temperature and dissolved O_2 levels of surface waters were measured every fifteen days during the study from October 2002 to May 2004. In the laboratory, precipitates were settled out and dried overnight at 45°C. After manually removing pieces of leaves and wood, the samples were disaggregated in an agate mortar.

A core sample was collected using a liquid nitrogen core-barrel system in the central main drain (sample b, Fig. 2), and then stored in a freezer (–18°C) until analysis. The core was cut into 2 cm slices and freeze-dried. The 2-cm thick slices were pooled together into 3 samples for the analyses in order to obtain enough material for chemical analyses and physical characterization.

Analytical methods

Bulk chemical analyses were obtained on 300 mg of dried representative sub-samples. The samples were digested in Teflon beakers on a heating plate using $LiBO_2$, and the residues were completely re-dissolved with HNO_3 before the analysis. Major elements were analysed by ICP-AES, total organic carbon (TOC) and total sulphur (TS) were determined using a LECO SC 144DRPC and trace elements analyses were performed by ICP-MS. International certified reference materials were used to check the entire analytical procedure, and detection limits are given in Table 1.

Powder X-ray diffraction (XRD) was carried out on a Philips instrument at 40 kV and 40 mA using a monochromator with CoK_α radiation, and scanning from 2.5 to 80.0 °2θ with a 0.015° step and 9 s counting time per step. In order to obtain more details about the 2-line Fh planes, XRD was also carried out from 25.0 to 50.0 °2θ and from 67.0 to 76.0 °2θ , with a 0.01° step and 20 s counting time per step.

^{57}Fe Mössbauer absorption spectra were recorded over the range ± 14 mm/s in 512 channels. The Mössbauer spectrometer was composed of a compact detector γ-system for high count-rates and a "Wissel" conventional constant acceleration Mössbauer device. A ^{57}Co (in Rh) source was used with a nominal activity of 50 mCi. The spectra were obtained at room temperature, specifically at 4 K to enhance the 2nd order Doppler effect, and then recorded on a multichannel Cambera analyzer coupled to a computer. The isomer shift was recorded with respect to α-Fe metal. Accord-

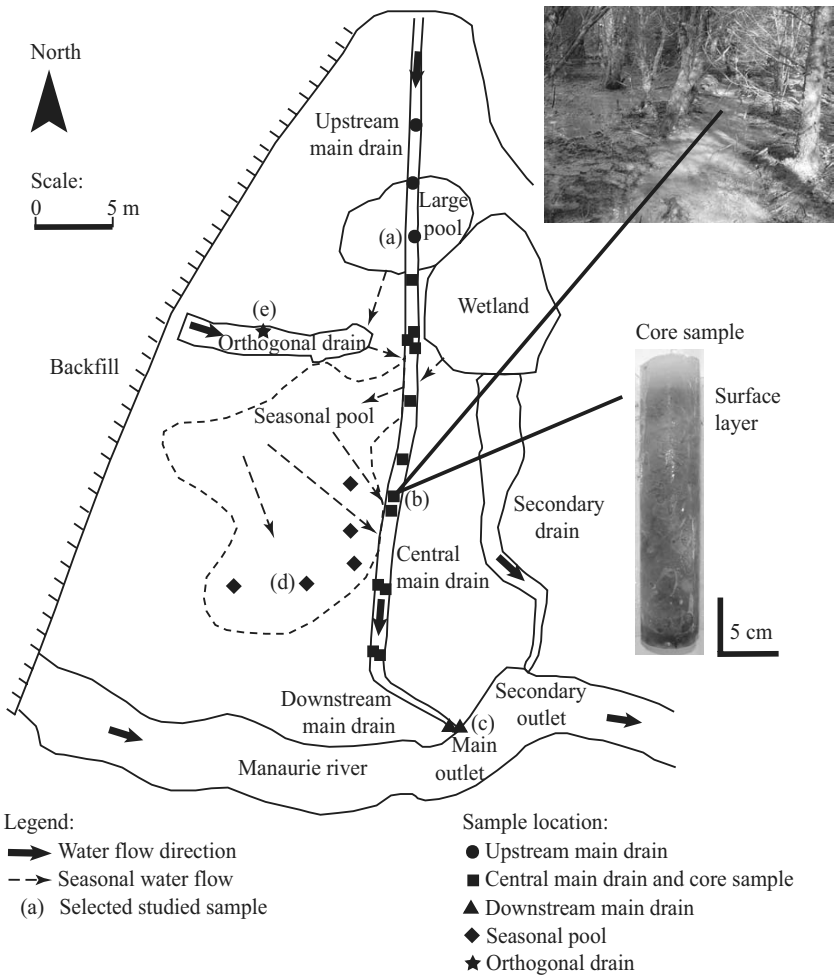

Fig. 2. Superficial and core sample location map. Letters correspond to selected studied samples used in the following figures: (a) Upstream main drain; (b) Central main drain; (c) Downstream main drain; (d) Seasonal pool; (e) Orthogonal drain.

ing to Rancourt *et al*. (1993), the absorber sample thickness for oxy-hydroxides can be approximated at around 100 mg of mineral per cm^2. Powders were finely ground under acetone and placed in a Plexiglas sample holder. Lorentzian line shapes were assumed for the deconvolutions, based on least-squares fitting procedures. χ^2 was used to measure the quality of the computer fit. Magnetically split spectra were fitted using hyperfine field distributions.

Differential thermal analyses (DTA) were performed using a Netzsch Thermal Analyser STA 409 EP, with the temperature range set at 25–1000°C and data acquired at a heating rate of 10°C/min in an ambient atmosphere. A 20-mg sample was used with alumina as the reference material.

Scanning Electron Microscope (SEM) was used at an accelerating voltage of 20 kV and with a focal distance of 10 mm on carbon-coated thin sections prepared from powder samples in hardened epoxy resin.

Results and discussion

Spatial evolution of iron oxide deposits

The median bulk chemical composition of the collected ochreous deposits is presented in Table 1. Samples are characterised by high Fe_2O_3 contents ranging from 29.2 to 57.2 wt %. They also contain high amounts of SiO_2, ranging from 1.7 to 33.4 wt %, Al_2O_3 (ranging from 0.2 to 9.8 wt %), TOC (up to 3.35 %), TS (up to 4.69 %) and As (ranging from 1 to 10 wt %). Arsenic contents in the solid fraction strongly depend on the sample location. Along the main drain, the median content decreases from 7.8 wt % for sample a to 1.2 wt % for sample c. Median contents for samples d and e (1.8 wt % and 1.9 wt %, respectively) are slightly higher than for sample c (see Fig. 2 for location).

The mineralogy of these ochreous deposits, determined by XRD, is dominated by Fh with traces of inherited minerals (mainly quartz, feldspar and clay minerals, Fig. 3) as indicated by the SiO_2 and Al_2O_3 contents (Fig. 3). The XRD patterns of Fh agree with those described by Cornell & Schwertmann (1996). The diffractogram of samples collected upstream (sample a, Fig. 3i) shows two very broad peaks near 1.49 Å and between 2.80 and 2.55 Å. These peaks correspond to the (300) and (110) planes of poorly crystalline 2-line Fh, called proto-Fh. The XRD pattern of samples collected downstream of the main drain (sample c, Fig. 3i) shows an additional weak peak at 1.97 Å. These samples can be called "poorly 2-line Fh" because they are better crystallised than proto-Fh (sample a). This indicates an increase of the mineral crystallinity from upstream to downstream along the main drain. An evolution can also be observed in the Fh crystallinity inside and outside the drain. Better crys-

Table 1. Bulk chemical compositions (ICP-MS and AES) of samples collected in the five studied areas, and also for core sample (see Fig. 2 for location).

		pH	SiO_2 wt%	Al_2O_3 wt%	Fe_2O_3 wt%	MnO wt%	MgO wt%	CaO wt%	Na_2O wt%	K_2O wt%	TiO_2 wt%	P_2O_5 wt%	TOC %	TS %	As wt%
Upstream main drain (a)	Median	5,7	5,1	2,6	40,9	0,1	0,2	0,39	0,1	0,6	0,11	0,37	0,12	1,92	7,8
	2σ	0,1	7,6	2,7	8	0	0,1	0,37	0,03	0,26	0,06	0,18	0,02	1,05	1,7
	n	3	3	3	3	3	3	3	3	3	3	3	3	3	3
Central main drain (b)	Median	6	6	2,8	45,9	0,2	0,2	0,48	0,31	0,36	0,09	0,2	0,32	2,44	3,1
	2σ	0,1	6,5	2,1	6,4	0,7	0,2	0,36	0,23	0,45	0,03	0,08	1,28	1,6	1,1
	n	11	11	11	11	11	11	11	11	11	11	11	11	11	11
Downstream main drain (c)	Median	6	31,1	5,5	30,1	0,4	0,4	0,7	0,86	1,7	0,1	0,17	1,88	0,15	1,2
	2σ	0	3,3	0,9	0,6	0	0,1	0,07	0,13	0,14	0,04	0,04	0,06	0,04	0,1
	n	2	2	2	2	2	2	2	2	2	2	2	2	2	2
Seasonal pool (d)	Median	6,3	8,2	2,7	41,2	0,4	0,2	0,5	0,22	0,48	0,13	0,17	0,21	3,3	1,8
	2σ	0	3,6	1,6	4,6	0,1	0	0,56	0,08	0,2	0,03	0,25	0,08	0,67	1,1
	n	5	5	5	5	5	5	5	5	5	5	5	5	5	5
Orthogonal drain (e)	n = 1	6	3,4	1,4	57,2	0,2	< d.l.	<d.l.	< d.l.	0,13	< d.l.	0,05	0,21	2,15	1,9
Core sample	0–8 cm*	6	6,2	2,7	51,1	0,2	< d.l.	0,45	< d.l.	0,28	0,05	0,18	2,39	0,24	1,1
	8–16 cm	–	12,1	4,9	45	0,3	0,3	0,38	0,16	0,61	0,11	0,22	3,05	0,18	0,9
	16–22 cm	–	14,3	5,7	42,1	0,3	0,3	0,35	0,15	0,78	0,13	0,23	3,35	0,17	0,7
d.l.		0,1	0,2	0,1	0,1	0,1	0,1	0,01	0,05	0,05	0,05	0,05	0,01	0,01	0,1

2σ: standard deviation, n: number of samples, –: not analysed, d.l.: detection limit, * values in cm correspond to the sample depth from the surface. Letters in () correspond to sample location (see Fig. 2).

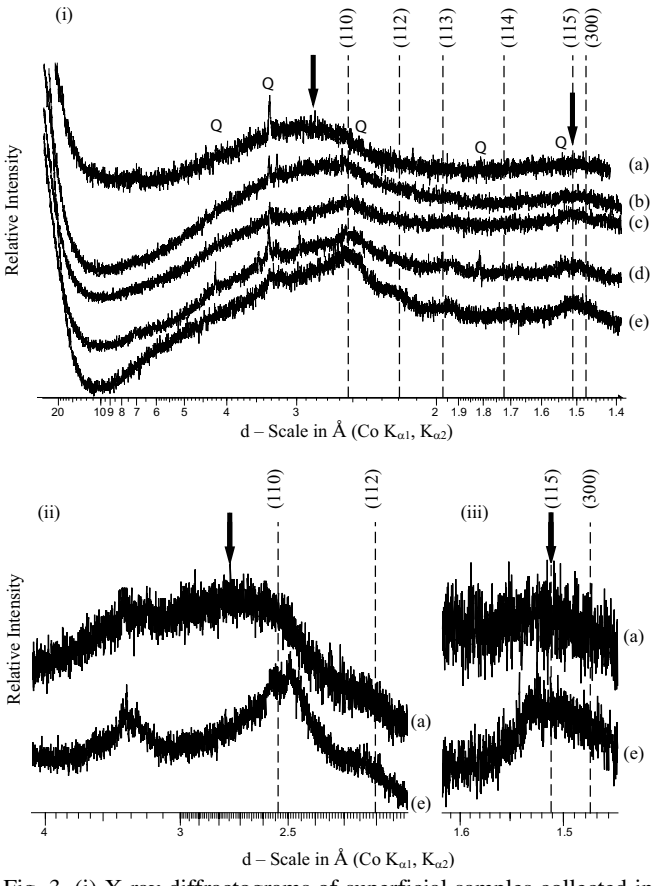

Fig. 3. (i) X-ray diffractograms of superficial samples collected in the 5 studied areas (a to e); (ii) and (iii) correspond to the (110) and (115) planes of Fh, respectively. Q=quartz; dashed lines and arrows correspond to the 6- and 2-line Fh positions, respectively. (See text for analytical conditions).

tallized Fh, called "better 2-line Fh", is observed in seasonal pools (sample d , Fig. 3i) with an additional weak peak at 1.97 Å corresponding to the (113) plane. The best crystallised Fh sample, also called "better 2-line Fh", is observed in the orthogonal drain (sample e, Fig. 3i). It is characterized by sharpened peaks and additional small broad peaks at 2.19 and 1.97 Å (Fig. 3i). The (110) and (115) reflections for sample e are sharper than for sample a, corresponding to the Fh crystallinity increase (Fig. 3ii and 3iii). No other iron oxide (goethite or hematite) was identified.

For samples located in the main drain (b and c, n = 13), a significant correlation ($r^2 = 0.90$) was observed between Fe and As in the solid fraction (Fig. 4). Arsenic concentration is highly dependent on Fe concentration, indicating that As is either adsorbed onto the Fh surface as complexes and/or coprecipitated in the Fh structure. X-ray elemental distributions obtained by SEM on thin sections show that Fe and As are located on the same particles, whereas S is strongly dispersed, indicating the absence in the material of any sulphidic As-bearing phases such as pyrite and arsenopyrite (Fig. 5). This observation confirms the affinity between Fe and As, but it provides no additional information about As coprecipitation and/or adsorption onto Fh. Specific attention is required for samples located in the upstream main drain (samples a in the grey-shaded domain, Fig. 4) since they do not follow the As-Fe correlation. In fact, these samples (category a; n = 3) contain higher amounts of As than samples b and c for a similar Fe content, according to the described correlation. This could be related to the crystallinity of the Fh: the least crystalline Fh has the highest As content (sample a, Fig. 3). In some cases, Fh crystallinity depends strongly on the elements in its structure such as As (Karim, 1984; Saleh & Jones, 1984; Eggleton & Fitzpatrick, 1988; Krause & Ettel, 1989; Drits *et al.*, 1993; Carlson *et al.*, 2002 and Schwertmann *et al.*, 2004). With decreasing As content in

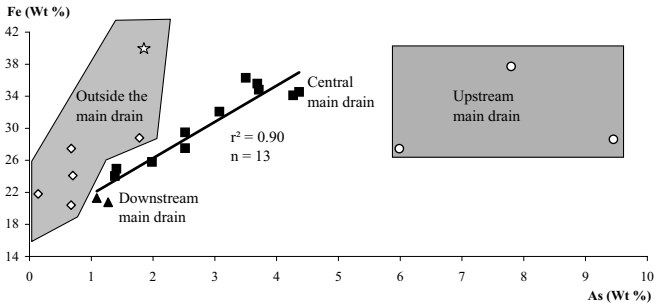

Fig. 4. Correlation of Fe (wt %) and As (wt %) for superficial samples. Open circles: samples (a), filled squares: samples (b), filled triangles: samples (c), open diamonds: samples (d), open stars: sample (e), (see Fig. 2 for sample location).

Fh, the XRD-peak corresponding to the (110) plane shifts from 2.80 to 2.53 Å, indicating a higher crystallinity of Fh (arrows in Fig. 3) as already shown by Krause & Ettel (1989) and Carlson *et al.* (2002). These samples (a, b and c) exhibit an evolution of crystallinity from proto-Fh upstream to poorly 2-line Fh downstream of the main drain. This evolution takes place by aqueous transformation (Jambor & Dutrizac, 1998; Cornell & Schwertmann, 1996) because the samples are always submerged, with an As decrease from 7.8 to 1.2 wt % (in the bulk solid composition, Table 1) as observed in the correlation (Fig. 4).

Samples located outside the drain and in the orthogonal drain (samples d and e, respectively, Fig. 2) do not belong to the correlation. These samples (dashed field, Fig. 4) contain less As for a similar range of Fe and are subject to a marked crystalline evolution (better 2-line Fh) compared to samples located in the main drain (samples b and c). The different states of crystallinity can be accounted for essentially in terms of As concentrations (Carlson *et al.*, 2002) and Fh transformation (Jambor & Dutrizac, 1998; Cornell & Schwertmann, 1996). These samples, located outside the main drain, are subject to dry episodes, with agglomeration and compaction, which explain why their evolution occurs by dry thermal transformation. Although samples d and e are the best crystallised samples, they contain higher As concentrations than expected in view of the crystallinity of samples b and c. However, since these samples are transformed during dry episodes, dry thermal transformation can be considered to have a weaker impact on the decrease of As in the solid. The observed decrease in As as a function of the increase in Fh crystallinity implies that As is coprecipitated in the Fh structure rather than adsorbed on the Fh surface.

Mössbauer spectroscopy was used in order to obtain information about the Fh chemical bonding (particle size, crystallinity, *etc.*). Mössbauer spectra of Fh show considerable variation due to different crystallinity or impurities (Cornell & Schwertmann, 1996). The Mössbauer spectra of the studied samples show a paramagnetic doublet at room temperature (291 K) and at 80 K (not shown). At 4 K, all spectra are completely magnetically split and appear as sextets, indicating that the Fe (III) spins are completely frozen

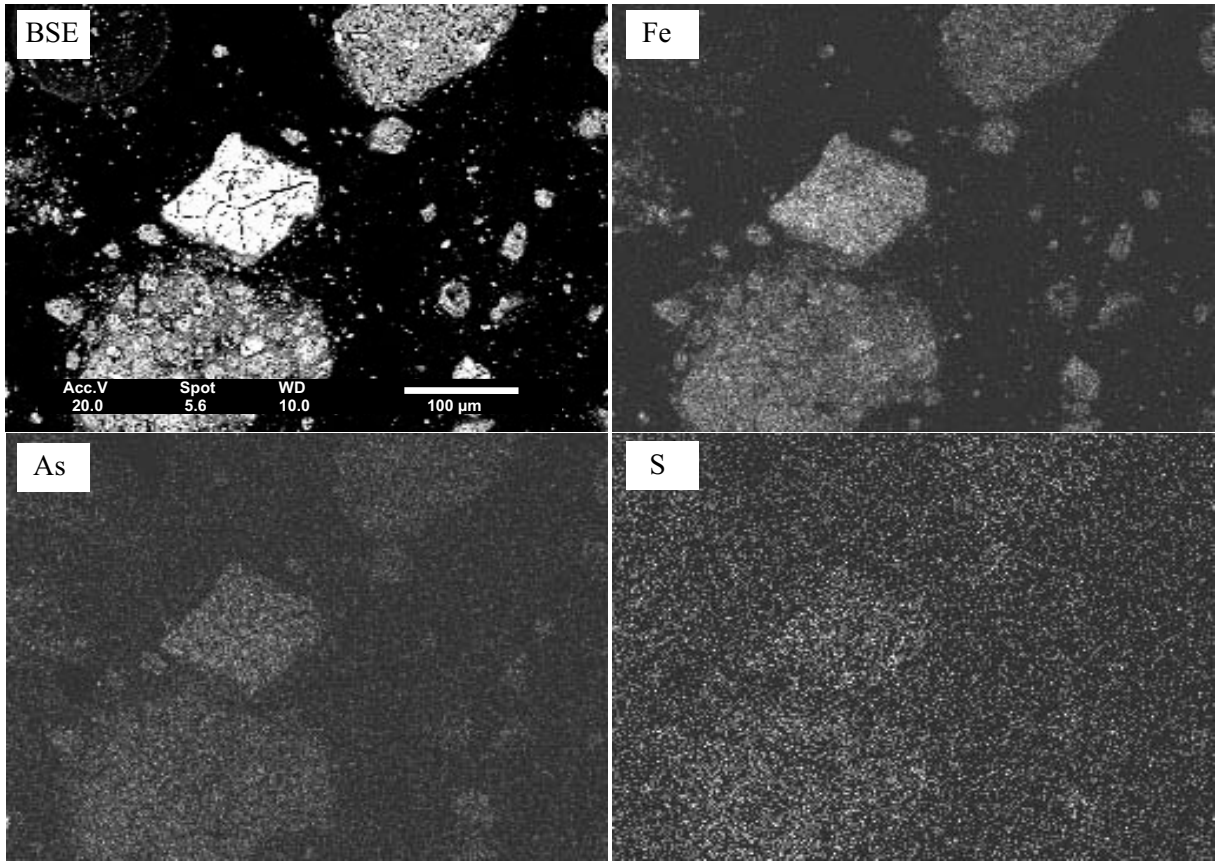

Fig. 5. Backscattered scanning electron microscope images of Fh powder in epoxy resin (thin sections coated with C) and associated elemental X-ray mapping for Fe, As and S of a sample collected in the central main drain (b).

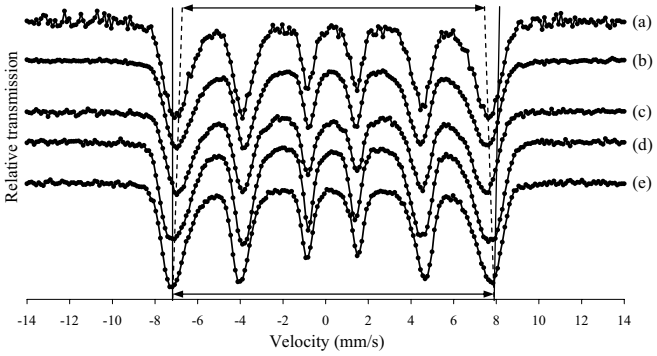

Fig. 6. Mössbauer spectra at 4 K of samples (a) to (e). Dashed lines indicate the increase of Fh crystallinity with the increase in the calculated B Hyperfine Field.

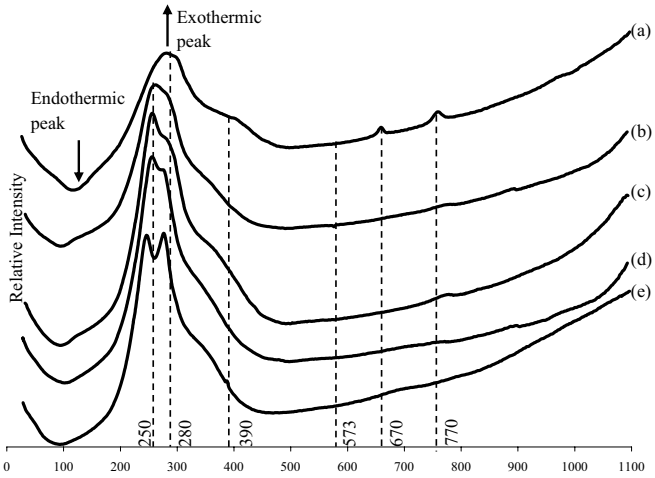

Fig. 7. Differential thermal analysis curves of superficial samples (a) to (e). Dashed lines indicate endothermic and exothermic peaks.

even in the most disordered oxide (Fig. 6, sample a). The isomer shift (IS) values range from 0.28 to 0.36 mm/s, which correspond to proto-Fh and better 2-line Fh respectively (Table 2). IS average values (with a mean of 0.33 mm/s) for the natural studied samples are similar to values for natural and synthetic Fh obtained by Murad & Schwertmann (1980).

The low quadrupole splitting (QS), less than 0.1 mm/s (average QS = –0.030 mm/s at 4 K, Table 2) and magnetic hyperfine field (Bhf) are characteristic of Fh (Cornell & Schwertmann, 1996). Moreover, IS and QS values correspond to a particle size less than 10 nm, which can be expected for natural poorly crystalline Fh (Carlson & Schwertmann, 1981; Schwertmann & Fisher, 1973; Schwertmann *et al.*, 2004). The adsorption of any species depends on the particle size, which determines the surface area of the adsorbing substrate. Jambor & Dutrizac (1998) determined the particle size of Fh aggregates to be 3–10 nm, with a high specific surface area ranging from 200 to 720 m^2/g. Due to the small size of the particles analysed by Mössbauer spectroscopy, a significant fraction of the bulk composition of Fh always represents the stoichiometry of the surface rather than the stoichiometry of the inner Fh structure. This could explain why As is not only coprecipitated in the Fh structure as assumed, but also forms part of the As adsorbed onto the Fh surface.

Bhf values are calculated using the distances between the external peaks of Mössbauer spectra, which show a weak increase from 45.4 to 46.8 T with increased crystallinity (Fig. 6 and Table 2). Due to the high As content of natural Fh, the Bhf determined in the studied samples is a little lower than the values obtained by Cornell & Schwertmann (1996). Similarly, other incorporated elements such as Si result in a decrease of the Bhf at 4.2 °K from 49.4 to 46.7 T as the Si content rises from 11.7 to 74.7 g/kg (Schwertmann *et al.*, 2004). High concentrations of Si and Al in the bulk analyses (Table 1) explain the observed slight Bhf increase in the studied samples. Half-widths and maxima of sextet exterior peaks, characterised by dashed lines in Fig. 6, shift to higher values as the particle size and crystallinity decrease. Due to the nanoparticle size distribution, the peaks are asymmetric. This indicates that the crystallinity of Fh increases with increasing Bhf. Spectra are characterised by asymmetric sextets towards lower velocities showing a range of hyperfine fields (Fig. 6), as shown by Zhao *et al.* (1994). Because Si, Al and C do not cause significant distortions of the Fe^{3+} environments (Rea *et al.*, 1994; Rancourt *et al.*, 2001), As can also be responsible for the QS increase and associated changes in the Fe^{3+} local environment (Fig. 6 and Table 2).

Thermoanalysis gives information about the Fh transformation and weight loss during heating. The obtained differential thermograms for the samples are typical of Fh (Fig. 7) as observed by Schwertmann & Fischer (1973) and Carlson & Schwertmann (1981). The thermal dehydration and dehydroxylation reactions of the different forms of oxy-hydroxides take place over a wide range of temperatures, usually depending on the nature of the compounds, the crystallinity and the chemical impurities. In this study, Fh spectra show an intense endothermic peak near 100°C, which results from a decrease in the high amount of adsorbed water contained in Fh (Fig. 7; Cornell & Schwertmann, 1996). The endothermic peak for better 2-line Fh (95°C) is broader than for proto-Fh (115°C), which is in agreement with Eggleton & Fitz-

Table 2. Mössbauer parameters measured at 4 K for the selected superficial Fh.

Locality	Oxide crystallinity	Isomer shift* (mm/s)	Average quadrupole splitting (mm/s)	B Hyperfine field (T)
Upstream main drain (a)	Proto-Fh	0,28	–0,03	45,4
Central main drain (b)	Proto-Fh	0,29	–0,03	45,5
Downstream main drain (c)	Poorly 2-line Fh	0,3	–0,03	45,5
Seasonal pool (d)	Better 2-line Fh	0,29	–0,03	45,8
Orthogonal drain (e)	Better 2-line Fh	0,36	–0,03	46,8

* referred to αFe metal

patrick (1988) who observed that 6-line Fh looses water more readily than less porous 2-line Fh. The As enrichment of proto-Fh causes a delayed release of water explaining the shift of the endothermic peak towards higher temperature (Fig. 3 and 5). Zhao *et al.* (1994) confirmed this process, showing that the adsorbed anions inhibit both the release of chemisorbed water molecules at low temperature (110°C) and the formation of hematite. The occurrence of As can also have an inhibiting effect at higher temperature when interfering with Fh formation during chain-building processes, as has been mentioned by Waychunas *et al.* (1993) and Manceau (1995). Such chain-building processes correspond to the polymerization of the octahedrally-coordinated iron (III) sheets, which induces the transformation to hematite (Carlson & Schwertmann, 1981).

The weak and broad exothermic peak near 280°C for proto-Fh is sharpened and resolved into two peaks (250 and 280°C) for better 2-line Fh (Fig. 7). The peak at 280°C shifts slightly at lower temperature with the increase of Fh crystallinity. The second exothermic peak at 250°C, not observable for proto-Fh, increases with even stronger intensity for better 2-line Fh. The twin exothermic peaks (250 and 280°C) are interpreted as the crystallisation of hematite (Schwertmann & Fischer, 1973; Schwertmann, 1979; Colombo & Violante, 1996; Cornell & Schwertmann, 1996). These peaks, generally observed between 300 and 350°C for pure Fh, shift to 280°C with increasing amount of Al (Colombo & Violante, 1996). Some of the following possibilities could explain the occurrence of this twin exothermic peak in the better crystallized 2-line Fh: (i) due to the presence of elements such as Si and Al, the first exothermic peak at 250°C is attributed to the transformation of highly disordered hematite, and the second, at 280°C, to the formation of better-ordered hematite (Cornell & Schwertmann, 1996); (ii) the first peak could be the result of maghemite growth and the second represents the conversion to hematite (Eggleton & Fitzpatrick, 1988); (iii) it could be attributed to a two-step crystallisation of hematite due to the presence of two different types of Fh crystalline structure present in the collected samples. However, Eggleton & Fitzpatrick (1988) observed this twin exothermic peak at 350 and 465°C, so the second possibility can be ruled out. Due to higher As contents in proto-Fh, the third possibility is more appropriate than the first one. Thus, the conversion to ordered hematite by recrystallisation is less rapid compared to a better 2-line Fh. The exothermic peak at 390°C shifts from 360 to 415°C with decreasing Fh crystallinity, indicating a transformation from Fh to maghemite as described by Eggleton & Fitzpatrick (1988). The shoulder near 390°C observed by Schwertmann & Fischer (1973) cannot be attributed to TOC content (Table 1), because TOC content does not correlate with the increase of the shoulder.

Weak and sharp exothermic peaks at 670 and 770°C were only observed in samples collected upstream of the main drain (Fig. 7). The first exothermic peak seems to be due to transformation of the poorly crystalline Al-associated Fh to hematite as consequence of high Al content (Table 1; Carlson & Schwertmann, 1981; Schwertmann, 1979). The exothermic peak at 770°C is caused by Si that prevents transformation to hematite, resulting in an elevated conversion temperature (Carlson & Schwertmann, 1981; Cornell & Schwertmann, 1996). This is because part of the H_2O is replaced by Si to form stronger Fe-O-Si bonds, thus delaying Fh transformation (Zhao *et al.*, 1994). The weak endothermic peak at 573°C (Table 1 and Fig. 3) corresponds to the transformation of α-quartz to β-quartz (Klimesch & Ray, 1997).

As discussed above, two kinds of Fh transformation can occur: (i) aqueous transformation for samples a, b and c (Torrent & Guzman, 1982; Schwertmann & Murad, 1983; Manceau & Drits, 1993) and (ii) dry thermal transformation for samples d and e (Carlson & Schwertmann, 1981; Eggleton & Fitzpatrick, 1988; Zhao *et al.*, 1994; Stanjek & Weidler, 1992). These transformations account for the observed different states of Fh crystallinity and its As content in the main drain. The occurrence of Si, delaying the Fh transformation, could explain why the range of As contents for samples outside the main drain is higher than the expected range.

Vertical evolution of iron oxide deposits

To study the vertical evolution in Fh chemistry and crystallinity, a core sample was collected in the main drain (Fig. 2). The As content decreases from 1.1 to 0.7 wt % with increasing depth from 0 to 22 cm (Table 1). This decrease in As correlates with the decrease of Fe_2O_3 and S_{tot}, ranging from 51.1 to 42.1 wt % and from 0.24 to 0.17 wt %, respectively. The simultaneous increase of other major elements (mainly SiO_2) is confirmed by the presence of silicate minerals (Fig. 8).

The 0–8-cm layer corresponds to proto-Fh, similarly to superficial samples taken in the central main drain (Fig. 3, b). With increasing depth, no vertical evolution in crystallinity could be observed by XRD (Fig. 8). The core sample located in the main drain was always submerged, and dry thermal transformation did not occur. Moreover, the parameters involved in the aqueous transformation (pH, ionic strength) do not vary significantly, which explains the lack of vertical evolution in Fh crystallinity. DTA curves of Fh core samples are similar to superficial samples taken in the main drain (Fig. 9). The endothermic peak near 100°C, which characterises proto-Fh, is broader in the core sample than in superficial samples collected at the same location (Fig. 9). There is no observable shifting of the twin exothermic peaks (close to 270°C) with increasing temperature (Fig. 9). Moreover, the first of the two exothermic peaks for Fh near 270°C does not change with depth in the core samples. This is similar to the superficial samples and expresses the lack of Fh evolution. This observation characterises a proto-Fh that can be transformed into highly-disordered hematite by heating, as seen in the thermal analyses of all the superficial samples. However, these three samples correspond to bulk samples and not to single samples, which may average out the shifting. This also explains the presence of only one exothermic peak rather than the two peaks observed for the superficial sample taken at the same location. Moreover, the vertical evolution is less marked and the Fh core samples contain less As than the superficial samples (decreasing by a factor of 2 from 10510 to 6450 ppm in the core, and by a factor of 10 from 77970 to 6898 ppm in the superficial samples). Thus, the shoulder near 370°C for the core samples does not

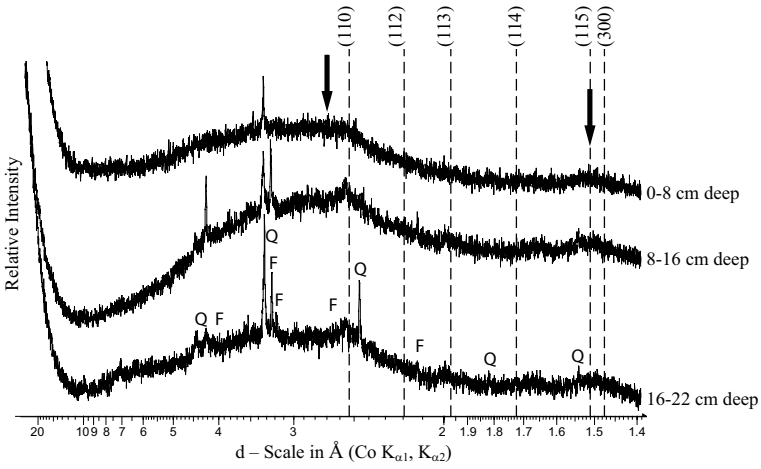

Fig. 8. X-ray diffractograms of different layers of the core sample. F=feldspar; Q=quartz; dashed lines and arrows correspond to the 6- and 2-line Fh positions, respectively.

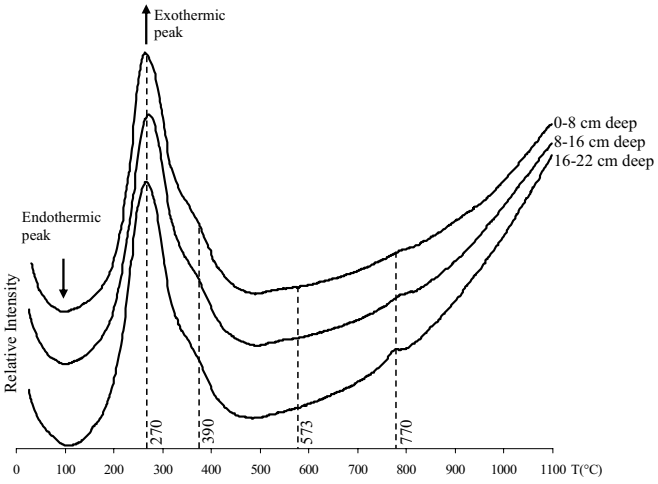

Fig. 9. Differential thermal analysis curves for different layers of the core sample. Dashed lines indicate endothermic and exothermic peaks.

shift as observed in the superficial samples, so it corresponds to the transformation from Fh to maghemite. The exothermic peak near 770°C increases with depth and depends on the Si content of the Fh (Fig. 9). The endothermic peak at 573°C characterises the occurrence of quartz in these samples (Klimesch & Ray, 1997), which is more abundant in the deeper samples (Fig. 8).

Summary – Conclusions

Fh deposits of different crystallinity were observed depending on the *in situ* conditions. In the main drain, Fh evolution from proto-Fh to poorly crystallized 2-line Fh occurs due to aqueous transformation, which is mainly controlled by water composition (pH, ionic strength, and redox potential). In the orthogonal drain and in the seasonal pool, dry thermal transformation is responsible for the formation of a better crystallized 2-line Fh than the Fh located in the main drain. This dry thermal transformation is linked to variations of air temperature, humidity, agglomeration and compaction. The evolution of crystallinity due to dry thermal transformation is more pronounced than in the evolution by aqueous transformation.

Furthermore, during the study, no stable Fe (III) oxide such as hematite or goethite was noted in the field. The weak evolution in crystallinity of 2-line Fh is related to the high As contents in the collected samples. Arsenic acts as an inhibitor of the transformation of Fh into more stable forms, which explains the absence of better crystallized iron oxide. According to the thermal analysis results, there are probable traces of Si and Al associated with the Fh, which could also account for the inhibition of Fh transformation into these stable forms.

In addition to the variable inputs of dissolved As according to the correlation, the As content (up to 10 wt %) in the solids seems to be related to (i) Fh crystallinity, with the better 2-line Fh tending to contain lower solid As concentrations; and (ii) Fh evolution by aqueous or dry thermal transformation, the latter producing a less marked decrease in As. The evolution of Fh crystallinity as a function of decreasing As suggests that it may be coprecipitated within the Fh structure. However, due to its small particle size and its high specific surface area, part of the As could also be adsorbed onto the Fh structure.

Although Fh contains high amounts of As, the methods used in these investigations yield insufficient information about the relationship between As and Fh. To provide additional information, TEM and EXAFS spectroscopy studies are in progress on the crystallographic structure of Fh, to address the short-term risks of potential As contamination due to As release into the environment.

Acknowledgements: We thank the associate editors and referees for their perceptive reviews of the manuscript. We would like to express our gratitude towards the European Social Funds and the Limousin Region for their financial support of this study. We gratefully acknowledge Michel Peymirat, Céline Boissard and Claude Fontaine of HydrASA (Limoges and Poitiers, France) for their technical and chemical assistance and the Laboratoire de Chimie de Coordination (Toulouse, France) for the Mössbauer spectroscopy analyses.

References

Appelo, C.A.J., Van der Weiden, M.J.J., Tournassat, C., Charlet, L. (2002): Surface complexation of ferrous iron and carbonate on

ferrihydrite and the mobilization of arsenic. *Env. Sci. Tech.*, **36**, 3096-3103.

Bigham, J.M., Schwertmann, U., Trana, S.J., Winland, R.L., Wolf, M. (1996): Schwertmannite and the chemical modeling of iron on acid sulfate water. *Geochim. Cosmochim. Acta*, **60**, 2111-2121.

Bouchot, V., Gros, Y., Bonnemaison, M. (1989): Structural controls on the auriferous shear zones of the Saint Yrieix District, Massif Central, France: evidence from the Le Bourneix and Laurieras gold deposits. *Econ. Geol.*, **84**, 1315-1327.

Carlson, L. & Schwertmann, U. (1981): Natural ferrihydrites in surface deposits from Finland and their association with silica. *Geochim. Cosmochim. Acta*, **45**, 421-429.

Carlson, L., Bigham, J.M., Schwertmann, U., Kyek, A., Wagner, F. (2002): Scavening of As from acid mine drainage by schwertmannite and ferrihydrite: a comparison with synthetic analogues. *Env. Sci. Tech.*, **36**, 1712-1719.

Cathelineau, M., Boiron, M.C., Holliger, P., Marion, P., Denis, M. (1989): Gold in arsenopyrites: crystal chemistry, location and state, physical and chemical conditions of deposition. *Econ. Geol.*, **84**, 328-341.

Chukhrov, F.V. (1973): On mineralogical and geochemical criteria in the genesis of red beds. *Chemical Geol.*, **12**, 67-75.

Colombo, C. & Violante, A. (1996): Effect of time and temperature on the chemical composition and crystallization of mixed iron and aluminum species. *Clays Clay Miner.*, **44**, 113-120.

Cornell, R.M. & Schwertmann, U. (1979): Influence of organic anions on the crystallization of ferrihydrite. *Clays Clay Miner.*, **27**, 402-410.

–,– (1996): The iron oxides. Structure properties, reactions, occurrence and uses. VCH, Weinheim, 573 p.

Dold, B. (2003): Dissolution kinetics of schwertmannite and ferrihydrite in oxidized mine samples and their detection by differential X-ray diffraction (DXRD). *Appl. Geochem.*, **18**, 1531-1540.

Drits, V.A., Shakarov, B.A., Salyn, A.L., Manceau, A. (1993): Structural model for ferrihydrite. *Clays Clay Miner.*, **28**, 185-207.

Eggleton, R.A. & Fitzpatrick, R.W. (1988): New data and a revised structural model for ferrihydrite. *Clays Clay Miner.*, **36**, 111-124.

Fuller, C.C., Davis, J.A., Waychunas, G.A. (1993): Surface chemistry of ferrihydrite: Part 2. Kinetics of arsenate adsorption and coprecipitation. *Geochim. Cosmochim. Acta*, **57**, 2271-2282.

Jambor, J.L. & Dutrizac, J.E. (1998): Occurrence and constitution of natural and synthetic ferrihydrite, a widespread iron oxyhydroxide. *Chem. Rev.*, **98**, 2549-2585.

Jang, J.H., Dempsey, B.A., Catchen, G.L., Burgos, W.D. (2003): Effects of Zn (II), Cu (II), Mn (II), Fe (II), NO_3^-, or SO_4^{2-} at pH 6.5 and 8.5 on transformations of hydrous ferric oxide (HFO) as evidenced by Mössbauer spectroscopy. *Colloids Surf., A*, **221**, 55-68.

Karim, Z. (1984): Characteristics of ferrihydrites formed by oxidation of $FeCl_2$ solutions containing different amounts of silica. *Clays Clay Miner.*, **32**, 181-184.

Klimesch, D.S. & Ray, A. (1997): The use of DTA/TGA to study the effects of ground quartz with different surface areas in autoclaved cement: quartz pastes. Use of the semi-isothermal thermogravimetric technique. *Thermochim. Acta*, **306**, 159-165.

Krause, E. & Ettel, V.A. (1989): Solubilities and stabilities of ferric arsenate compounds. *Hydrometallurgy*, **22**, 311-337.

Manceau, A. (1995): The mechanism of anion adsorption on iron oxides: evidence for the bonding of arsenate tetrahedra on free Fe(O, OH)6 edges. *Geochim. Cosmochim. Acta*, **59**, 3647-3653.

Manceau, A. & Drits, V.A. (1993): Local structure of ferrihydrite and feroxyhite by EXAFS spectroscopy. *Clay Miner.*, **28**, 165-184.

Martinez, C.E. & McBride, M.B. (1999): Dissolved and labile concentrations of Cd, Cu, Pb, and Zn in aged ferrihydrite-organic matter systems. *Env. Sci. Tech.*, **33**, 745-750.

Murad, E. & Schwertmann, U. (1980): The Mössbauer spectrum of ferrihydrite and its relations to those of other iron oxides. *Am. Mineral.*, **65**, 1044-1049.

Nicaud, J. (2001): Contrôle structural de la mise en place des minéralisations aurifères du district de Saint-Yrieix-La-Perche (Massif Central français): analyse de la fracturation et étude des altérations hydrothermales. Thèse de doctorat, Université de Limoges, 252 p.

Rancourt, D.G., McDonald, A.M., Lalonde, A.E., Ping, J.Y. (1993): Mössbauer absorber thickness for accurate site populations in Fe-bearing minerals. *Am. Mineral.*, **78**, 1-7.

Rancourt, D.G., Fortin, D., Pichler, T., Thibault, P.J., Lamarche, G., Moris, R.V., Mercier, P.H.J. (2001): Mineralogy of a natural As-rich hydrous ferric oxide coprecipitate formed by mixing of hydrothermal fluid and seawater: implication regarding surface complexation and color banding in ferrihydrite deposits. *Am. Mineral.*, **86**, 834-851.

Rea, B.A., Davis, J.A., Waychunas, G.A. (1994): Studies of the reactivitiy of the ferrihydrite surface by iron isotopic exchange and Mössbauer spectroscopy. *Clays Clay Miner.*, **42**, 23-24.

Saleh, A.M. & Jones, A.A. (1984): The crystallinity and surface characteristics of synthetic ferrihydrite and its relationship to kaolinite surfaces. *Clay Miner.*, **19**, 745-755.

Schwertmann, U. (1979): The influence of aluminum on iron oxides: 5. Clay minerals as source of aluminum. *Soil Sci.*, **128**, 195-200.

Schwertmann, U. & Fischer, W.R. (1973): Natural "amorphous" ferric hydroxide. *Geoderma*, **10**, 237-247.

Schwertmann, U. & Murad, E. (1983): Effect of pH on the transformation of goethite and hematite from ferrihydrite. *Clays Clay Miner.*, **31**, 277-284.

Schwertmann, U., Friedl, J., Kyek, A. (2004): Formation and properties of a continuous crystallinity series of synthetic ferrihydrites (2- to 6-line) and their relation to FeOOH forms. *Clays Clay Miner.*, **52**, 221-226.

Stanjek, H. & Weidler, P.G. (1992): The effect of dry heating on the chemistry, surface area, and oxalate solubility of synthetic 2-line ad 6-line ferrihydrites. *Clay Miner.*, **27**, 397-412.

Torrent, J. & Guzman, R. (1982): Crystallization of Fe(III)-oxides from ferrihydrite in salt solutions: osmotic and specific ion effects. *Clay Miner.*, **17**, 463-469.

Vempati, R.K. & Loeppert, R.H. (1989): Influence of structural and adsorbed Si on the transformation of synthetic ferrihydrite. *Clays Clay Miner.*, **37**, 273-279.

Waychunas, G.A., Rea, B.A., Fuller, C.C., Davis, J.A. (1993): Surface chemistry of ferrihydrite: Part 1. EXAFS studies of the geometry of coprecipitated and adsorbed arsenate. *Geochim. Cosmochim. Acta*, **57**, 2251-2269.

Zhao, J., Huggins, F.E., Feng, Z., Huffman, G.P. (1994): Ferrihydrite: surface structure and its effects on phase transformation. *Clays Clay Miner.*, **42**, 737-746.

Received 9 March 2005
Modified version received 5 May 2005
Accepted 27 October 2005